Visualization of Multichannel EEG Coherence Networks Based on Community Structure

Ji, Chengtao; Maurits, N.M.; Roerdink, Jos B.T.M.

Published in:
6th International Conference on Complex Networks and Their Applications, Nov 29–Dec 1, Lyon, France

DOI:
10.1007/978-3-319-72150-7_47

Visualization of Multichannel EEG Coherence Networks Based on Community Structure Analysis

Chengtao Ji[1(✉)], Natasha M. Maurits[2], and Jos B. T. M. Roerdink[1]

[1] Johann Bernoulli Institute for Mathematics and Computer Science, University of Groningen, Groningen, The Netherlands
{c.ji,j.b.t.m.roerdink}@rug.nl
[2] Department of Neurology, University Medical Center Groningen, University of Groningen, Groningen, The Netherlands
n.m.maurits@umcg.nl

Abstract. An electroencephalography (EEG) coherence network is a representation of functional brain connectivity. However, typical visualizations of coherence networks do not allow an easy embedding of spatial information or suffer from visual clutter, especially for multichannel EEG coherence networks. In this paper, a new method for data-driven visualization of multichannel EEG coherence networks is proposed to avoid the drawbacks of conventional methods. This method partitions electrodes into dense groups of spatially connected regions. It not only preserves spatial relationships between regions, but also allows an analysis of the functional connectivity within and between brain regions, which could be used to explore the relationship between functional connectivity and underlying brain structures. In addition, we employ an example to illustrate the difference between the proposed method and two other data-driven methods when applied to coherence networks in older and younger adults who perform a cognitive task. The proposed method can serve as an preprocessing step before a more detailed analysis of EEG coherence networks.

1 Introduction

EEG records the electrical activity of the brain by attaching electrodes to the scalp of a subject at multiple locations. Synchronous electrical activity in brain regions is generally assumed to imply functional integration. Such synchronization occurs over a large range of scales. A large number of methods have been proposed to measure the synchrony between pairs of brain regions, and these measures are often closely correlated [21]. EEG coherence is one of these measures, which is calculated between pairs of electrode signals as a function of frequency [13,16].

An EEG coherence network represents functional brain connectivity, more precisely, the coherences between pairs of signals recorded by the electrodes.

C. Cherifi et al. (eds.), *Complex Networks & Their Applications VI*,
Studies in Computational Intelligence 689, https://doi.org/10.1007/978-3-319-72150-7_47

Visualization of coherence networks plays an important role as a preprocessing step in the exploration of brain connectivity [8]. It can provide insight into unexpected patterns of brain functioning and help neuroscientists to understand how the brain works, especially for the case where no *a priori* assumptions or hypotheses about brain activity in specific regions are made. However, visualization of high-density or multichannel EEG (at least 64 electrodes) coherence networks is not always managed well [8]. Typical visualizations of coherence networks are a matrix representation with rows and columns representing electrodes with cells representing coherences between electrode signals or a node-link diagram with vertices representing electrodes and edges representing coherences. However, such representations can suffer from some drawbacks. The matrix representation is effective for visualizing large and/or dense networks, but the relative spatial location is hard to embed; the node-link diagram could preserve spatial information to some extent, but it suffers from the potentially large number of overlapping edges when visualizing dense networks.

To study connectivity patterns in the coherence graph, researchers often employ a hypothesis-driven or semi-data-driven definition of certain regions of interest (ROIs), in which all electrodes are assumed to record similar signals because of volume conduction effects [12,15]. However, these methods generally depend on certain assumptions or hypotheses.

As an alternative to the hypothesis-driven and semi-data-driven approaches, ten Caat *et al.* [6–8] proposed a method for detection of data-driven ROIs, referred to as *functional units* (FUs). The maximal clique based (MCB) method of ten Caat *et al.* [6] focused on FUs defined as spatially connected maximal cliques, for which vertex sets are as large as possible. Since the MCB method [6] is very time-consuming, as an alternative a watershed based (WB) method was proposed that detects spatially connected cliques in a greedy way [7]. To reduce the potential over-segmentation of this approach, an improved watershed based method (IWB) was proposed [8]. The FUs detected by the IWB method are similar but not identical to the FUs detected by the MCB method. To distinguish them we therefore denote the corresponding FUs by $\mathrm{FU}^{\mathrm{MCB}}$ and $\mathrm{FU}^{\mathrm{IWB}}$, respectively.

A drawback of the MCB and IWB methods is that the analysis of local synchronization is difficult, since these methods detect maximal cliques, that is, groups of spatially-connected electrodes that are as large as possible.

Therefore, in this paper we propose an alternative, based on network *community structure* [18]. The proposed method, referred to as the community clique-based (CCB) method, partitions the set of electrodes into several data-driven ROIs (communities) based on their connections and positions to find the most relevant brain regions. As a result, electrodes within the same community are spatially connected and are more densely connected than electrodes in different communities. For brevity, the ROIs obtained by community detection will still be called "functional units", but denoted by the symbol $\mathrm{FU}^{\mathrm{CCB}}$ to distinguish them from the functional units obtained by the MCB and IWB methods.

Overall, the new community-based method for detecting functional units is not only expected to reduce the drawbacks of the conventional hypothesis-based approaches, but also to allow a more detailed analysis of the relationship between functional connectivity and underlying brain structure than the data-driven MCB and IWB methods.

2 Related Work

The principal concept in our approach is to visualize brain connectivity, and to extract meaningful information from this representation for further analysis. The challenge in visualization often lies in the analysis of a huge amount of data, in our case the large number of EEG channels.

A straightforward method would be to visualize functional brain connectivity data as 3D node-link diagrams: ROIs are shown as nodes and the relationships between these nodes are encoded in the edges. But this approach suffers from visual clutter, and side effects of 3D rendering such as occlusion are hard to remedy [3,10].

An alternative approach is to depict the connectivity data by a 2D representation, which could reduce the work of 3D rendering. A wide variety of methods has been developed to map data on 2D space to visualize neuronal interactions or relations between brain regions. To preserve the spatial information of the data to some extent, a node-link diagram based on a biologically meaningful layout has been used [1]. In this biological layout, planar projections are used for the 3D electrode locations on the surface of a head. Vertices are usually mapped according to a top view of the head, sometimes to two separate side views of the left and right hemispheres. However, such a visualization with edges representing connections may suffer from a large number of overlapping edges, resulting in a cluttered representation, especially for a large amount of data.

Some methods were proposed to remedy the visual clutter by eliminating overlaps and reducing the number of long-distance edges employing graph drawing. For example, for 2D node-link diagrams the layout can be calculated by multidimensional scaling or force-directed algorithms [11]. However, such methods usually change the layout of the vertices to reduce visual clutter. Yet, the spatial context of the data is still vital for facilitating the interpretation of the data by neuroscientists. Hence, node-link diagrams are often accompanied by a separate picture showing the position of nodes, with nodes on the two representations being matched by color encoding or labeling [17]. In this approach, information about spatial context is not presented in a single image. Matrix representations are also popular to represent functional connectivity networks. This approach outperforms the node-link diagram in visualizing large networks. By arranging ROIs along the rows and columns of a matrix, their spatial relations are, however, lost [14].

3 Method

3.1 EEG Coherence

During an EEG experiment, brain activity is recorded by electrodes attached to the scalp of a subject at different locations. The degree of interaction between two electrode signals can be measured by coherence which is a measure for the similarity of signals as a function of frequency. The coherence c_λ as a function of frequency λ for two continuous time signals x and y is defined as the absolute square of the cross-spectrum f_{xy} normalized by the autospectra f_{xx} and f_{yy} [13], having values in the interval [0, 1]: $c_\lambda(x, y) = \frac{|f_{xy}(\lambda)|^2}{f_{xx}(\lambda) f_{yy}(\lambda)}$.

3.2 Data Representation and EEG Coherence Network

A network is simply a collection of connected objects. We refer to the objects as nodes or vertices and the connections between the nodes as edges. In mathematics, networks are often referred to as *graphs*. In this paper, we use the terms *network* and *graph* interchangeably.

Table 1. Coherence Matrix. Values above or equal to the significance threshold, in this case 0.2, are indicated in bold.

	a	b	c	d	e	f	g	h	i	j	k	l
a	k0	**0.65**	0.10	0.10	**0.64**	**0.60**	**0.20**	0.10	**0.30**	**0.23**	0.10	0.10
b	**0.65**	0	0.10	0.10	**0.63**	**0.63**	**0.21**	0.10	**0.32**	**0.33**	0.10	0.10
c	0.10	0.10	0.10	0	0.10	0.10	0.10	0.10	0.10	0.10	0.10	0.10
d	0.10	0.10	0.10	0	0.10	0.10	**0.70**	**0.71**	0.10	0.10	0.10	**0.70**
e	**0.64**	**0.63**	0.10	0.10	0	**0.62**	**0.20**	0.10	**0.33**	**0.20**	0.10	0.10
f	**0.60**	**0.63**	0.10	0.10	**0.62**	0	**0.70**	0.10	**0.30**	**0.31**	0.10	0.10
g	**0.20**	**0.21**	0.10	**0.70**	**0.20**	**0.70**	0	**0.69**	**0.20**	**0.20**	0.10	**0.70**
h	0.10	0.10	0.10	**0.71**	0.10	0.10	**0.69**	0	0.10	0.10	0.10	**0.72**
i	**0.30**	**0.32**	0.10	0.10	**0.33**	**0.30**	**0.20**	0.10	0	**0.32**	0.10	0.10
j	**0.23**	**0.33**	0.10	0.10	**0.20**	**0.31**	**0.20**	0.10	**0.32**	0	0.10	0.10
k	0.10	0.10	0.10	0.10	0.10	0.10	0.10	0.10	0.10	0.10	0	0.10
l	0.10	0.10	0.10	**0.70**	0.10	0.10	**0.70**	**0.72**	0.10	0.10	0.10	0

Functional brain connectivity obtained from EEG data is represented by an undirected *coherence graph* $G = (V, E)$, defined by a set of vertices V and a set of edges $E \subseteq V \times V$ where vertices represent electrodes. Since weak coherences may represent spurious connections and these connections tend to obscure the topology of strong and significant connections [22], we only consider coherences with values above a pre-defined significance threshold [8,13]. Coherences

above the significance threshold are represented by edges, whereas coherences below the threshold are ignored (see Fig. 1(c)); see Table 1. Vertices are not self-connected. To determine spatial relationships between electrodes, a Voronoi diagram is employed, which partitions the plane into regions of points with the same nearest vertex (for a simple example, see Fig. 1(a)). For EEG data, the vertex set is equal to the set of electrode positions. The vertices are referred to as (Voronoi) centers, and the region boundaries as (Voronoi) polygons. The area enclosed by a polygon is called a (Voronoi) cell. We call two cells *Voronoi neighbors* if they have a boundary in common. A collection of cells C is called Voronoi connected if for a pair $\phi_0, \phi_n \in C$, there is a sequence $\phi_0, \phi_1, ..., \phi_n$ of cells in C, with each pair ϕ_{i-1}, ϕ_i consisting of Voronoi neighbors. Cells, vertices, nodes, and electrodes are interchangeable in this paper.

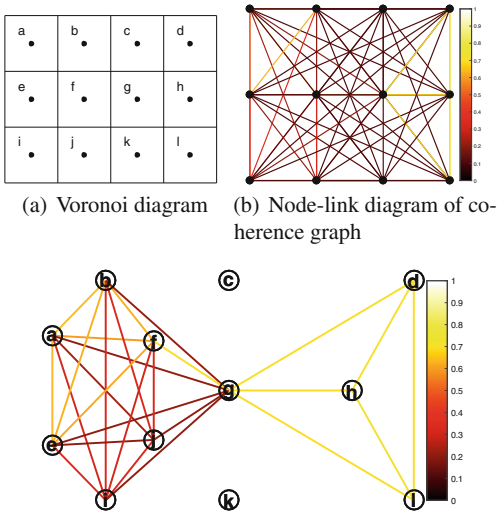

(a) Voronoi diagram (b) Node-link diagram of coherence graph

Fig. 1. Example layout of a coherence network with coherence matrix as shown in Table 1. (a) Voronoi diagram showing vertex positions with vertex labels within the cells and Voronoi connections between vertices. Vertices are spatial neighbors if they are 4-connected, e.g., the spatial neighbors of vertex f are vertices, b, e, g, and j. (b) Layout preserving the vertex positions. Vertices are represented by solid circles and lines represent coherences between vertices, while the coherence values are encoded by the color of the lines (see the color bar on the right). (c) Manual layout of the significant coherence graph without considering the vertex positions.

3.3 Community Clique Detection

3.3.1 Community Structure

The community structure of a network is defined as a grouping of nodes in a set of groups (communities), with a high density of within-group connections

and a lower density of between-group connections. Such structures have been observed in many different types of networks including social, biological, and tele-communication networks [9,19]. In particular, the community structure of a brain functional connectivity network shows the groups of neuronal areas where there is more synchronous activity within a group and less synchronous activity between groups. These communities may be considered as functional areas in the brain [2].

Various algorithms have been proposed for the identification of community structure from complex networks. Many of these algorithms are based on the idea of optimizing the *modularity index* Q of the partition of a network [19,20]. In the case of a weighted network, this index is defined as follows [4]:

$$Q = \frac{1}{2m} \sum_{v,v'} \Big[c(v,v') - \frac{K_v K_{v'}}{2m} \Big] \delta(L(v), L(v')) \tag{1}$$

where $c(v,v')$ represents the weight (in our case the coherence value) of the edge between nodes v and v', $K_v = \sum_l c(v,l)$ is the sum of weights of the edges incident to vertex v, $L(v)$ is the community label of vertex v, the function $\delta(i,j)$ is 1 if $i = j$ and 0 otherwise, and $m = \frac{1}{2} \sum_{v,v'} c(v,v')$.

3.3.2 Community Clique Detection Method

A simple and efficient method of optimizing modularity was proposed by Blondel *et al.* [4]. Here, we extend this method to obtain dense spatially-connected cliques, the community clique, consisting of Voronoi-connected vertices of the EEG coherence network.

The outline of our method can be summarized as follows. The difference with Blondel's method is in step 2, the calculation of the modularity gain, where an extra condition is applied which ensures that the resulting communities are spatially connected cliques (see the introduction for the motivation):

1. Assign a unique community to each node of the network.
2. Use Eq. 2 to calculate the modularity gain ΔQ for node v caused by removing node v from its community and placing it in another community *such that the node v is connected to each node of that community and has at least one Voronoi neighbour in that community.*
3. Place the node v in the community for which the gain is the highest and positive. If no positive gain is available, nothing is done.
4. Continue repeating steps (2) and (3) until every node is processed.
5. Repeat steps (2) -(4) until no further improvement of the modularity index Q is achieved.

The following equation is used to calculate the modularity gain ΔQ when removing one node v from its community $C_{L(v)}$ to an arbitrary community C_i [4, 22,23]:

$$\Delta Q = \frac{1}{2m} \Big(\sum_{l \in C_i} c(v,l) - \sum_{l \in C_{L(v)}} c(v,l) - \frac{K_v (\sum_{C_i} - \sum_{C_{L(v)}} + K_v)}{2m} \Big) \tag{2}$$

where $\sum_{C_{L(v)}}$ is the sum of the weights of the links incident to nodes in $C_{L(v)}$, $\sum_{C_i}$ is the sum of the weights of the links incident to nodes in C_i, and K_v is the sum of the weights of the links incident to node v.

Note that the algorithm's output depends on the order in which the nodes are processed in step 2. The ordering does not have a significant influence on the modularity that is obtained, but can influence the computation time [4]. In our case, a decreasing order is chosen based on the average local coherence of vertices, which is also used to detect basins in the IWB method [8]. For a data set of 119 electrodes, the computing time was around 0.84 s on a modern desktop computer (Intel 3.2Ghz, 8GB RAM).

Figure 2 illustrates the procedure of community clique detection for an EEG coherence network, with the coherence matrix shown in Table 1. The following detailed description contains references to Fig. 2.

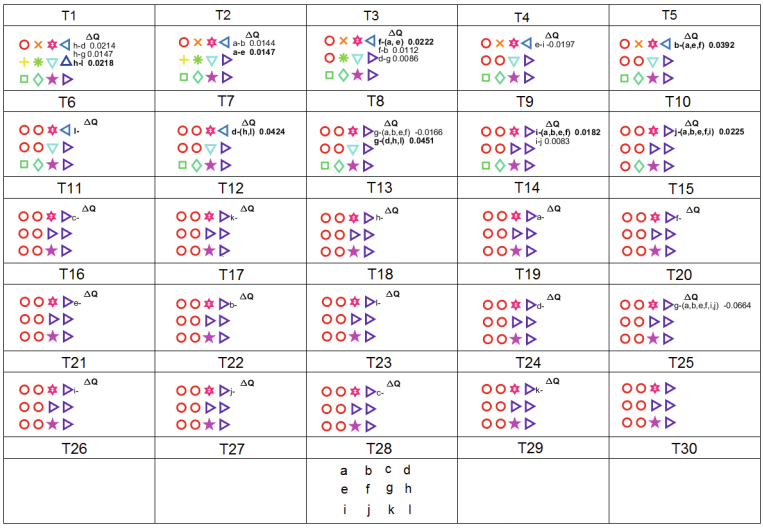

Fig. 2. Illustration of Voronoi-connected community clique detection for a coherence network with the coherence matrix shown in Table 1. Each colored symbol represents a community at **T1**. For each step **Ti**, the gain ΔQ is shown on the right. Before the dash: the node to be removed; after the dash: the node or nodes constituting a community. **T28** shows the vertex positions in 2D space.

At **T1**, the initial stage, each of these twelve vertices correspond to a unique community represented by a specific colored symbol: $L(a) = 1$, $L(b) = 2$, $L(c) = 3$, $L(d) = 4$, $L(e) = 5$, $L(f) = 6$, $L(g) = 7$, $L(h) = 8$, $L(i) = 9$, $L(j) = 10$, $L(k) = 11$, $L(l) = 12$. Then, we calculate the modularity gain ΔQ caused by removing k (since k has the highest local average coherence, and the descending order of vertices based on their local average coherence is: $h, a, f, e, b, l, d, g, i, j, c, k$) from its community to the other communities; all the values of ΔQ are listed

on the right in Fig. 2. **T2-T12**. At every next step, the next vertex v will be chosen and the gain of removing v from its community $C_{L(v)}$ to the remaining communities will be computed. If the positive highest gain $max\Delta Q$ results from the movement of node v to the community in which v has at least one Voronoi neighbour and is connected with each vertex in that community, then the vertex v will be removed from its original community to the destination community C_{Des}, $C_{L(v)}$ is updated by deleting v from $C_{L(v)}$ and C_{Des} is replaced by the union of itself with v. At **T2**, $v = h$, $C_{L(v)} = C_8 = \emptyset$, $C_{Des} = C_{12} = \{h, l\}$. At **T3**, $v = a$, $C_{L(v)} = C_1 = \emptyset$, $C_{Des} = C_5 = \{a, e\}$. At **T4**, $v = f$, $C_{L(v)} = C_6 = \emptyset$, $C_{Des} = C_5 = \{a, e, f\}$. At **T5**, $v = e$, nothing is done since $max\Delta Q$ is negative when merging e and i into one community. At **T6**, $v = b$, $C_{L(v)} = C_2 = \emptyset$, $C_{Des} = C_5 = \{a, b, e, f\}$. At **T7**, $v = l$, nothing is done since all the communities except C_{12}, the original community, have no connected Voronoi neighbours of l. At **T8**, $v = d$, $C_{L(v)} = C_4 = \emptyset$, $C_{Des} = C_{12} = \{d, h, l\}$. At **T9**, $v = g$, $C_{L(v)} = C_7 = \emptyset$, $C_{Des} = C_{12} = \{g, d, h, l\}$. At **T10**, $v = i$, $C_{L(v)} = C_9 = \emptyset$, $C_{Des} = C_5 = \{a, b, e, f, i\}$. At **T11**, $v = j$, $C_{L(v)} = C_{10} = \emptyset$, $C_{Des} = C_5 = \{a, b, e, f, i, j\}$. At **T12**, $v = c$, and at **T13**, $v = k$, nothing is done since the vertex v has no connected Voronoi-neighbours.

From **T14** on, all vertices will be traversed again. The gain ΔQ can be easily computed and it can be observed that there is no more positive gain, which means the modularity can not be improved anymore. So the detection procedure stops. Finally, we obtain two community cliques $\{a, b, e, f, i, j\}$ and $\{g, d, h, l\}$ at **T25**.

3.4 FU Visualization

The functional units detected by the CCB method are visualized in an FU^{CCB} (functional unit) map, in exactly the same way as for the FU^{MCB} and FU^{IWB} maps. Spatial groups of similarly colored (in gray scale) cells correspond to FUs with a size of at least four, while white cells are part of smaller FUs. Circles overlayed on the cells represent the barycenters of the FUs and are connected by lines whose color reflects the average coherence between all electrodes of the FUs. See [6] for details. In addition, we use the colour of the circle over the geographic centre of FU C_1 to reflect its *average coherence* $\hat{c}_\lambda(C_1)$, which is defined as $\hat{c}_\lambda(C_1) = \frac{\sum_{i,j}\{c_\lambda(v_i,v_j)|v_i \in C_1, v_j \in C_1\}}{|C_1|(|C_1|-1)}$. See Fig. 3 for examples of FU map visualization.

4 Results

4.1 Experimental Setup

Brain responses were recorded during an auditory oddball detection experiment (For further detail, see [8]. A *significance threshold* for the estimated coherence is then given by Halliday *et al.* [13]: $\theta = 1 - p^{1/(L-1)}$, where p is a probability value associated with a confidence level α, such that $p = 1 - \alpha$. Throughout this section, we use $p = 0.01$, and $L = 13$ segments. In addition, we set the inter-FU coherence threshold to the same value as the significance threshold θ.

4.2 FU Maps

FU maps for two participants are shown in Fig. 3.

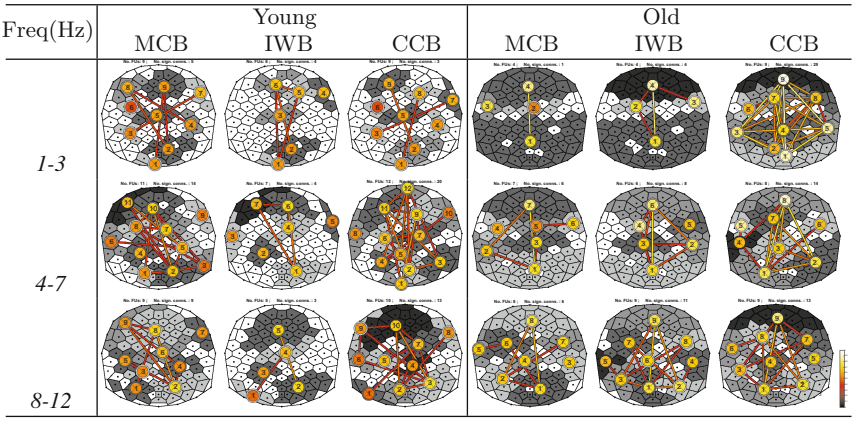

Fig. 3. Illustration of FU maps (top view, nose on top) obtained by using the three FU detection methods for three different EEG frequency bands. Data obtained from a young participant with corresponding FU maps in the first three columns, and from an older participant with corresponding FU maps in the last three columns.

We make the following observations:

1. For the young participant, it can be observed that the MCB and CCB methods detect similar numbers of FUs and connections between FUs in the frequency bands of [1–3]Hz and [4–7]Hz. The number of connections between FUs in the frequency band [8-12]Hz is clearly more different.
2. For the old participant, in the frequency band of [1–3] Hz, large differences occur between the FU maps obtained by the three different methods. The MCB method detects two large FUs located anteriorly and posteriorly, with significant inter-FU coherence between them. The IWB method has a similar result, except for the frontal-central connection. The CCB method finds a total of nine FUs with size above four. Compared to the CCB method, FU ***1*** obtained by the MCB and IWB methods is split into five FUs ***1, 2, 3, 4, 5*** in the CCB method due to the weak inter-community connections with each other. FU^{CCB}***1*** in the CCB method has the highest average coherence among these 5 FUs, and electrodes of this FU^{CCB} are distributed over both left and right parietal-occipital regions of the brain. This means there is a high interhemispheric coherence, which decreases at the central-parietal areas, as can be seen from the average coherence of FU^{CCB}***4*** and the inter-FU coherence between FU^{CCB}***3*** and FU^{CCB}***5***. The FU^{CCB}***2*** and FU^{CCB}***4*** in the central-parietal areas of the brain have a lower average coherence compared to the FU^{CCB}***1, 3, 5***. In addition, the inter-FU coherences between FU^{CCB}***1, 3, 5***

are larger than the inter-FU^{CCB} coherences between ***2, 4*** and ***1, 3, 5***. From a global view, the two FUs^{CCB} having the strongest connection are ***1*** and ***9***, which are located at the frontal and parietal-occipital areas of the brain, respectively. The next largest inter-FU coherence occurs between FUs^{CCB} ***1, 9*** and FUs^{CCB} ***3, 5***; that is, the parietal-temporal area of the brain is more synchronized with the frontal and parietal-occipital areas of the brain.

3. In the frequency band of [4-7] Hz for the old participant, the MCB and IWB methods have similar results, except in the frontal-central area of the brain. Because the IWB method is an approximation of MCB, we only compare the MCB and CCB methods here. The main difference is that the FU^{MCB} ***1*** of the MCB method is split into FUs^{CCB} ***1*** and ***2*** in the CCB method due to weak inter-community connections. The FUs^{CCB} **1, 2** have a high coherence with the FU^{CCB} **8** located at the frontal area of the brain, and FU^{CCB} **8** has the highest average coherence among the FUs detected by the CCB method. In the mid line of the brain, there are two large FUs^{CCB} **3, 7**, which means that electrodes within FUs^{CCB} **3, 7** are more coherent with each other. We also observe that FU^{CCB} **3** is spatially close to FUs^{CCB} **1, 2** but their inter-FU coherence is less than the inter-FU coherence between FU^{CCB} **8** and FUs^{CCB} **1, 2**.
4. Again for the old participant, in the frequency band of [8-12] Hz, more FUs and connections between FUs appear in the MCB and IWB methods compared with the lower frequency bands. In this frequency band, the three methods tend to have similar results, particularly for the MCB and IWB method. The three methods share an almost similar FU (FU^{MCB} **8**, FU^{IWB} **9**, FU^{CCB} **9**, which is located frontally). The largest difference between methods is in the composition of the FUs, which is caused by different FU-detection criteria.

In the CCB method, the older participant has higher local and global synchronization compared to the younger participant over three frequency bands, which is in accordance with Maurits *et al.* [16], i.e., higher interhemispheric coherence was found in the older subjects in the frequency band [1–3]Hz, and aging is associated with increased EEG coherence during a relatively easy cognitive task. It should be noted, however, that we here only discuss examples. Throughout the three frequency bands, FUs with high average coherence are found in frontal and parietal-occipital regions for the older participant. These FUs usually have high inter-FU coherence as well, in accordance with previous observations in the literature [5,8]. In contrast, FUs in the mid line are less synchronized. For the young participant, the FUs are generally less synchronized. The left- and right-temporal regions are less synchronized, as the average coherence of FUs are very low in our examples.

5 Conclusions and Future Work

Visualization is an important aspect in the analysis of EEG coherence, especially for multichannel EEG coherence networks. While conventional methods are either suffering from reduced spatial information or visual clutter, they have

inherent limitations when applied to EEG coherence networks. We developed a visualization approach based on the functional unit (FU) concept that attempts to preserve spatial relationships between functional brain regions and allows analysis of functional connectivity within and between regions.

This method first partitions an EEG coherence network into dense groups of spatially connected electrodes recording pairwise significantly coherent signals. The resulting communities (groups of electrodes) were visualized in an FU map, which makes it possible to investigate the relationship between functional brain connectivity and underlying brain structure. Results were compared to earlier FU detection methods based on maximal clique or improved watershed based algorithms. This comparison showed that there is a considerable difference for a strong coherence network, in which the CCB method detects more FUs compared to the MCB and IWB methods. For weak coherence networks, in which nodes are usually significantly connected with their neighbours while being less connected with nodes at a longer distance, the three methods detect FUs locally and the difference in the number of detected FUs decreases.

Our method is a visually aided pre-processing method that can be used before analysis questions about data are well defined. Although our method is specific to EEG coherence networks, we believe that it can be easily adapted to other network visualizations which need to capture the whole structure of networks and that do not only depend on the analysis of single nodes or specified connections between pairs of nodes.

Acknowledgments. C. Ji acknowledges the China Scholarship Council (Grant number: 201406240159) for financial support.

References

1. Achard, S., Salvador, R., Whitcher, B., Suckling, J., Bullmore, E.: A resilient, low-frequency, small-world human brain functional network with highly connected association cortical hubs. J. Neurosci. **26**(1), 63–72 (2006)
2. Ahmadlou, M., Adeli, H.: Functional community analysis of brain: a new approach for eeg-based investigation of the brain pathology. Neuroimage **58**(2), 401–408 (2011)
3. Alper, B., Bach, B., Henry Riche, N., Isenberg, T., Fekete, J.D.: Weighted graph comparison techniques for brain connectivity analysis. In: Proceedings of the SIGCHI Conference on Human Factors in Computing Systems, pp. 483–492. ACM (2013)
4. Blondel, V.D., Guillaume, J.L., Lambiotte, R., Lefebvre, E.: Fast unfolding of communities in large networks. J. Stat. Mech. Theory Exp. **2008**(10), P10,008 (2008)
5. ten Caat, M., Lorist, M.M., Bezdan, E., Roerdink, J.B.T.M., Maurits, N.M.: High-density EEG coherence analysis using functional units applied to mental fatigue. J. Neurosci. Methods **171**(2), 271–278 (2008)
6. ten Caat, M., Maurits, N.M., Roerdink, J.B.T.M.: Functional unit maps for data-driven visualization of high-density EEG coherence. In: Proceedings Eurographics/IEEE VGTC Symposium on Visualization (EuroVis), pp. 259–266 (2007)

7. ten Caat, M., Maurits, N.M., Roerdink, J.B.T.M.: Watershed-based visualization of high-density EEG coherence. In: Banon, G.J.F., Barrera, J., de Mendoca Braga-Neto, U. (eds.) Proceedings 8th International Symposium on Mathematical Morphology, Rio de Janeiro, pp. 289–300 (2007)
8. ten Caat, M., Maurits, N.M., Roerdink, J.B.T.M.: Data-driven visualization and group analysis of multichannel EEG coherence with functional units. IEEE Trans. Vis. Comput. Graph. **14**(4), 756–771 (2008)
9. Danon, L., Diaz-Guilera, A., Duch, J., Arenas, A.: Comparing community structure identification. J. Stat. Mech. Theory Exp. **2005**(09), P09,008 (2005)
10. Dosenbach, N.U., Nardos, B., Cohen, A.L., Fair, D.A., Power, J.D., Church, J.A., Nelson, S.M., Wig, G.S., Vogel, A.C., Lessov-Schlaggar, C.N., et al.: Prediction of individual brain maturity using fmri. Science **329**(5997), 1358–1361 (2010)
11. Fruchterman, T.M., Reingold, E.M.: Graph drawing by force-directed placement. Softw. Pract. Exp. **21**(11), 1129–1164 (1991)
12. Gladwin, T.E., Lindsen, J.P., de Jong, R.: Pre-stimulus eeg effects related to response speed, task switching and upcoming response hand. Biol. Psychol. **72**(1), 15–34 (2006)
13. Halliday, D.M., Rosenberg, J.R., Amjad, A.M., Breeze, P., Conway, B.A., Farmer, S.F.: A framework for the analysis of mixed time series/point process data-theory and application to the study of physiological tremor, single motor unit discharges and electromyograms. Prog. Biophys. Mol. Bio. **64**(2/3), 237–278 (1995)
14. Kamiński, M., Blinowska, K., Szelenberger, W.: Topographic analysis of coherence and propagation of eeg activity during sleep and wakefulness. Electroencephalogr. Clin. Neurophysiol. **102**(3), 216–227 (1997)
15. Lachaux, J.P., Rodriguez, E., Martinerie, J., Varela, F.J., et al.: Measuring phase synchrony in brain signals. Hum. Brain Mapp. **8**(4), 194–208 (1999)
16. Maurits, N.M., Scheeringa, R., van der Hoeven, J.H., de Jong, R.: Eeg coherence obtained from an auditory oddball task increases with age. J. Clin. Neurophysiol. **23**(5), 395–403 (2006)
17. Nelson, S.M., Cohen, A.L., Power, J.D., Wig, G.S., Miezin, F.M., Wheeler, M.E., Velanova, K., Donaldson, D.I., Phillips, J.S., Schlaggar, B.L., et al.: A parcellation scheme for human left lateral parietal cortex. Neuron **67**(1), 156–170 (2010)
18. Newman, M.E.: Fast algorithm for detecting community structure in networks. Phys. Rev. E **69**(6), 066,133 (2004)
19. Newman, M.E.: Finding community structure in networks using the eigenvectors of matrices. Phys. Rev. E **74**(3), 036,104 (2006)
20. Newman, M.E., Girvan, M.: Finding and evaluating community structure in networks. Phys. Rev. E **69**(2), 026,113 (2004)
21. Nunez, P.L., Srinivasan, R., Westdorp, A.F., Wijesinghe, R.S., Tucker, D.M., Silberstein, R.B., Cadusch, P.J.: Eeg coherency: I: statistics, reference electrode, volume conduction, laplacians, cortical imaging, and interpretation at multiple scales. Electroencephalogr. Clin. Neurophys. **103**(5), 499–515 (1997)
22. Rubinov, M., Sporns, O.: Complex network measures of brain connectivity: uses and interpretations. Neuroimage **52**(3), 1059–1069 (2010)
23. Sun, Y., Danila, B., Josić, K., Bassler, K.E.: Improved community structure detection using a modified fine-tuning strategy. EPL (Europhys. Lett.) **86**(2), 28,004 (2009)